Effect of external fields and currents on electronic nematic ordering with quadrupole moments

Satoru Hayami

Graduate School of Science, Hokkaido University, Sapporo 060-0810, Japan

Abstract

We theoretically investigate the effect of external fields and currents on electronic nematic orderings based on the concept of augmented multipoles consisting of electric, magnetic, magnetic toroidal, and electric toroidal multipoles. We show the relation between rank-2 electric quadrupoles and the other multipoles, the former of which corresponds to the microscopic order parameter for the nematic phases. The electric (magnetic) field induces the rank-1 and rank-3 electric (magnetic) multipoles and rank-2 electric toroidal (magnetic toroidal) quadrupoles, while the electric current induces the rank-1 and rank-3 magnetic toroidal multipoles and rank-2 magnetic quadrupoles. We classify the active multipoles under magnetic point groups, which will be a reference to explore cross-correlation and transport phenomena in nematic phases. As a demonstration, we show that unconventional symmetric and antisymmetric spin splittings are brought about by field-induced toroidal multipoles.

Keywords: multipole, nematic ordering, toroidal moment, cross-correlation response

1. Introduction

The orbital degree of freedom in electrons has attracted much interest in condensed matter physics, since it becomes a source of unconventional electronic orderings and their related physical phenomena [1, 2, 3]. Among them, electronic nematic orderings, which appear through the spontaneous breaking of rotational symmetry in solids, have been extensively studied in both theory and experiments [4, 5]. In contrast to magnetic orderings, the breaking of time-reversal ($\mathcal{T}$) symmetry is not necessary, and hence, qualitatively distinct low-energy excitations and physical phenomena are expected. The electronic nematic states have been discussed in various contexts, such as the Pomeranchuk instability [6, 7, 8], spin nematic state [9, 10, 11, 12, 13, 14, 15, 16], and charge/orbital nematic state [17, 18, 19, 20, 21, 22, 23], which have been studied

Email address: hayami@phys.sci.hokudai.ac.jp (Satoru Hayami)

in d-electron materials like iron-based superconductors [24, 25, 26, 27, 28, 29], $Sr_3Ru_2O_7$ [30, 31, 32], and Ba_2MgReO_6 [33, 34, 35] and f-electron materials, such as CeB_6 [36, 37, 38, 39], $PrPb_3$ [40, 41, 42], PrT_2X_{20} (T = Ir, Rh, X = Zn; T = V, X = Al) [43, 44, 45, 46, 47], and CeCoSi [48, 49, 50, 51, 52, 53, 54]. Recently, further exotic states coexisting spin and nematic orders have been suggested, such as the CP^2 skyrmion [55, 56, 57, 58] and other multiple-Q states [59, 60, 61, 62, 63].

The breaking of the rotational symmetry is related to the emergence of multipole moments, since the multipoles of rank 1 or higher describe the spatial anisotropy. The microscopic order parameter in the nematic state can be described by the multipole moment; the electric multipole characterized by the polar tensor with time-reversal even corresponds to the order parameter. For example, when the fourfold rotational symmetry of the tetragonal system in Fig. 1(a) is broken, the order parameter is expressed as the xy component of the electric quadrupole, $Q_{xy} \propto xy$, where the spatial charge distribution is shown in Fig. 1(b). Such an electric quadrupole breaks neither the spatial inversion ($\mathcal{P}$) symmetry nor $\mathcal{T}$ symmetry.

In the present study, we investigate the effect of the breakings of $\mathcal{P}$ and $\mathcal{T}$ symmetries under the electronic nematic orderings accompanying the electric quadrupole. Especially, we focus on further symmetry breakings by external fields and currents. Based on symmetry and microscopic multipole representation analyses [64, 65, 66], we show the coupling between rank-2 electric quadrupole and external stimuli. As a result, we find that external stimuli induce various multipole moments through $\mathcal{P}$ and/or $\mathcal{T}$ symmetry breakings; the electric (magnetic) field induces the electric (magnetic) dipoles and octupoles, and electric toroidal (magnetic toroidal) quadrupole, while the electric current induces the magnetic toroidal dipoles and octupoles, and magnetic quadrupoles. We discuss the relevant cross-correlation and transport properties in each case. Furthermore, we classify the symmetry lowering under these stimuli in terms of active multipoles. We also show the multipole couplings under external electric and magnetic fields for the atomic model as an example. In addition, we show the modification of the spin-split band structure under external fields, which can be experimentally detected in spin- and angle-resolved photoemission spectroscopy. Our systematic investigation will provide the possibility of not only acquiring functionalities related to the violation of $\mathcal{P}$ and $\mathcal{T}$ parities but also generating and controlling multipole moments under nematic orderings.

The rest of this paper is organized as follows. In Sect. 2, we show active multipoles induced by external fields and currents under electronic nematic orderings. Then, we classify such field-induced multipoles under magnetic point groups in Sect. 3. We discuss the multipole couplings in the presence of external fields by considering the atomic model in Sect. 4. We show that the field-induced magnetic toroidal and electric toroidal multipoles affect the symmetric and antisymmetric spin splittings in the band structure, respectively, in Sect. 5. Section 6 is devoted to a summary of this paper.

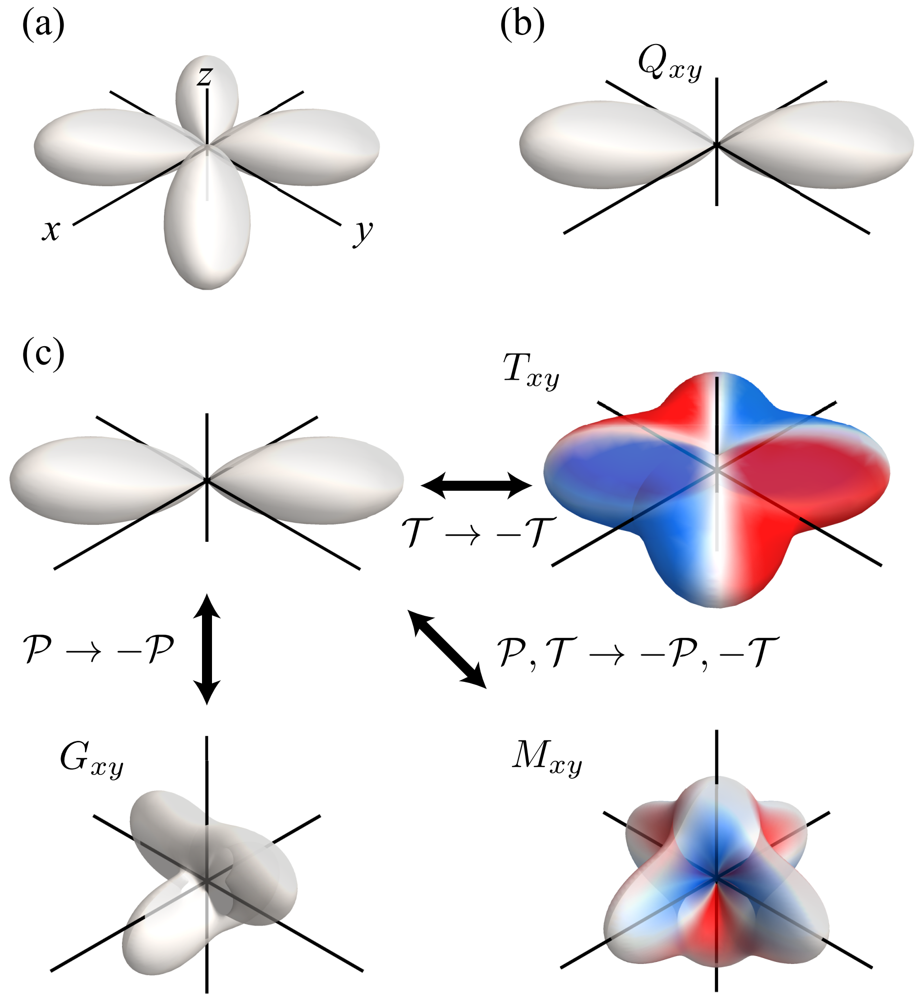

Figure 1: (a) Example of the orbital state under the tetragonal symmetry, where its shape represents the spatial charge distribution. (b) The charge distribution of the electric quadrupole Q_{xy}, which appears as a result of the breaking of fourfold rotational symmetry. (c) The conversion of the spatial inversion ($\mathcal{P}$) and time-reversal ($\mathcal{T}$) parities for Q_{xy}; the opposite $\mathcal{P}$ ($\mathcal{T}$) parity leads to the electric toroidal quadrupole G_{xy} (magnetic toroidal quadrupole T_{xy}), and the opposite $\mathcal{P}$ and $\mathcal{T}$ lead to the magnetic quadrupole M_{xy}. The red and blue colors represent the z component of the positive and negative orbital-angular momentum density, respectively.

2. Active multipoles under external fields and currents

In this section, we show what types of multipoles emerge by applying the external fields and currents to the nematic phases. We here focus on the electronic-origin nematic phases, which are induced by the ordering degrees of freedom in electrons by supposing that the lattice distortion through the phase transition is small. For that purpose, let us introduce four types of multipoles for later discussion. Four types of multipoles correspond to the electric multipole Q_{lm} with the $\mathcal{P}$ and $\mathcal{T}$ parities of $(\mathcal{P},\mathcal{T}) = [(-1)^l,+1]$, magnetic multipole M_{lm} with $(\mathcal{P},\mathcal{T}) = [(-1)^{l+1},-1]$, magnetic toroidal multipole T_{lm} with $(\mathcal{P},\mathcal{T}) = [(-1)^l,-1]$, and electric toroidal multipole G_{lm} with $(\mathcal{P},\mathcal{T}) = [(-1)^{l+1},+1]$, where l and m represent the rank of multipoles and its component. These four types of multipole with distinct $\mathcal{P}$ and $\mathcal{T}$ parities constitute a complete set in the Hilbert space in electron systems [67, 68]. In terms of the $\mathcal{P}$ and $\mathcal{T}$ parities, the electric multipole Q_{lm}, which are described by the spherical harmonics, is related to G_{lm} by reversing $\mathcal{P}$, T_{lm} by reversing $\mathcal{T}$, and M_{lm} by reversing both $\mathcal{P}$ and $\mathcal{T}$ [69, 64, 65]. For example, the counterparts of the electric quadrupole Q_{xy} in the other three multipoles are given by the electric toroidal quadrupole G_{xy}, magnetic toroidal quadrupole T_{xy}, and magnetic quadrupole M_{xy}, respectively, whose spatial distributions in terms of the charge and orbital-angular momentum densities are schematically shown in Fig. 1(c) [64]; it is noted that the $\mathcal{P}$ ($\mathcal{T}$) symmetry is lost in G_{xy} (T_{xy}), while both $\mathcal{P}$ and $\mathcal{T}$ symmetries are lost in M_{xy}.

Among these multipoles, the electric quadrupole $Q_{2m} = (Q_u, Q_v, Q_{yz}, Q_{zx}, Q_{xy}) \propto (3z^2-r^2, x^2-y^2, yz, zx, xy)$ under invariant $\mathcal{P}$ and $\mathcal{T}$ corresponds to the order parameter under electronic nematic orderings. For example, the spin-nematic order parameter $S_\alpha S_\beta$ for $\alpha,\beta = x,y,z$ is described by a linear combination of the electric quadrupole. In other words, the rotational symmetry breaking and its related directional-dependent physical phenomena are attributed to the appearance of Q_{2m}.

In the following, we show the coupling between the electric quadrupole and other multipoles via external fields and currents. First, we show the specific expressions of their coupling in Sect. 2.1. Then, we apply the results for the electric field in Sect. 2.2, the magnetic field in Sect. 2.3, and the electric current in Sect. 2.4.

2.1. Effect of vector fields

We consider the coupling between the electric quadrupole Q_{2m} and the external vector fields/currents $\boldsymbol{F} = (F_x, F_y, F_z)$ based on the group theory, which becomes sources of anisotropic responses. Since Q_{2m} and $\boldsymbol{F}$ correspond to the rank-2 and rank-1 quantities, their product leads to the rank-1 dipole, rank-2 quadrupole, and rank-3 octupole quantities, which are denoted by $(\mathcal{D}_x, \mathcal{D}_y, \mathcal{D}_z)$, $(\mathcal{Q}_u, \mathcal{Q}_v, \mathcal{Q}_{yz}, \mathcal{Q}_{zx}, \mathcal{Q}_{xy})$, and $(\mathcal{O}_{xyz}, \mathcal{O}^\alpha_x, \mathcal{O}^\alpha_y, \mathcal{O}^\alpha_z, \mathcal{O}^\beta_x, \mathcal{O}^\beta_y, \mathcal{O}^\beta_z)$, respectively.

The rank-1 dipole-type coupling is given by

$$\mathcal{D}_x = \left(-\frac{1}{\sqrt{3}}Q_u + Q_v\right) F_x + Q_{xy}F_y + Q_{zx}F_z, \tag{1}$$

$$\mathcal{D}_y = Q_{xy}F_x - \left(\frac{1}{\sqrt{3}}Q_u + Q_v\right) F_y + Q_{yz}F_z, \tag{2}$$

Table 1: The relationship between the external vector fields $\boldsymbol{F} = (F_x, F_y, F_z)$ and the rank-1–3 multipoles under the electric quadrupole (EQ) $Q_{2m} = (Q_u, Q_v, Q_{yz}, Q_{zx}, Q_{xy})$.

EQ	F_x	F_y	F_z
Q_u	$(\mathcal{D}_x,\, \mathcal{Q}_{yz},\, \mathcal{O}_x^{\alpha,\beta})$	$(\mathcal{D}_y,\, \mathcal{Q}_{zx},\, \mathcal{O}_y^{\alpha,\beta})$	$(\mathcal{D}_z,\, \mathcal{O}_z^{\alpha})$
Q_v	$(\mathcal{D}_x,\, \mathcal{Q}_{yz},\, \mathcal{O}_x^{\alpha,\beta})$	$(\mathcal{D}_y,\, \mathcal{Q}_{zx},\, \mathcal{O}_y^{\alpha,\beta})$	$(\mathcal{Q}_{xy},\, \mathcal{O}_z^{\beta})$
Q_{yz}	$(\mathcal{Q}_u,\, \mathcal{Q}_v,\, \mathcal{O}_{xyz})$	$(\mathcal{D}_z,\, \mathcal{Q}_{xy},\, \mathcal{O}_z^{\alpha,\beta})$	$(\mathcal{D}_y,\, \mathcal{Q}_{zx},\, \mathcal{O}_y^{\alpha,\beta})$
Q_{zx}	$(\mathcal{D}_z,\, \mathcal{Q}_{xy},\, \mathcal{O}_z^{\alpha,\beta})$	$(\mathcal{Q}_u,\, \mathcal{Q}_v,\, \mathcal{O}_{xyz})$	$(\mathcal{D}_x,\, \mathcal{Q}_{yz},\, \mathcal{O}_x^{\alpha,\beta})$
Q_{xy}	$(\mathcal{D}_y,\, \mathcal{Q}_{zx},\, \mathcal{O}_y^{\alpha,\beta})$	$(\mathcal{D}_x,\, \mathcal{Q}_{yz},\, \mathcal{O}_x^{\alpha,\beta})$	$(\mathcal{Q}_v,\, \mathcal{O}_{xyz})$

$$\mathcal{D}_z = Q_{zx}F_x + Q_{yz}F_y + \frac{2}{\sqrt{3}}Q_uF_z, \tag{3}$$

where $(\mathcal{D}_x, \mathcal{D}_y, \mathcal{D}_y)$ represent the nonuniform field distinct from the uniform field (F_x, F_y, F_z), which is referred to as an anisotropic dipole [70]. The rank-2 quadrupole-type coupling is given by

$$\mathcal{Q}_u = \sqrt{3}Q_{yz}F_x - \sqrt{3}Q_{zx}F_y, \tag{4}$$
$$\mathcal{Q}_v = Q_{yz}F_x + Q_{zx}F_y - 2Q_{xy}F_z, \tag{5}$$
$$\mathcal{Q}_{yz} = -(\sqrt{3}Q_u + Q_v)F_x - Q_{xy}F_y + Q_{zx}F_z, \tag{6}$$
$$\mathcal{Q}_{zx} = Q_{xy}F_x - (-\sqrt{3}Q_u + Q_v)F_y - Q_{yz}F_z, \tag{7}$$
$$\mathcal{Q}_{xy} = -Q_{zx}F_x + Q_{yz}F_y + 2Q_vF_z, \tag{8}$$

and the rank-3 octupole-type coupling is given by

$$\mathcal{O}_{xyz} = Q_{yz}F_x + Q_{zx}F_y + Q_{xy}F_z, \tag{9}$$
$$\mathcal{O}_x^{\alpha} = \sqrt{\frac{3}{5}}\left[\frac{\sqrt{3}}{2}(-Q_u + \sqrt{3}Q_v)F_x - Q_{xy}F_y - Q_{zx}F_z\right], \tag{10}$$
$$\mathcal{O}_y^{\alpha} = \sqrt{\frac{3}{5}}\left[-Q_{xy}F_x - \frac{\sqrt{3}}{2}(Q_u + \sqrt{3}Q_v)F_y - Q_{yz}F_z\right], \tag{11}$$
$$\mathcal{O}_z^{\alpha} = \sqrt{\frac{3}{5}}\left[-Q_{zx}F_x - Q_{yz}F_y + \sqrt{3}Q_uF_z\right], \tag{12}$$
$$\mathcal{O}_x^{\beta} = -\frac{1}{2}(\sqrt{3}Q_u + Q_v)F_x + Q_{xy}F_y - Q_{zx}F_z, \tag{13}$$
$$\mathcal{O}_y^{\beta} = -Q_{xy}F_x + \frac{1}{2}(\sqrt{3}Q_u - Q_v)F_y + Q_{yz}F_z, \tag{14}$$
$$\mathcal{O}_z^{\beta} = Q_{zx}F_x - Q_{yz}F_y + Q_vF_z, \tag{15}$$

where the overall numerical coefficient is appropriately taken in each rank for notational simplicity. $\mathcal{D}$, $\mathcal{Q}$, and $\mathcal{O}$ denote any of electric multipole Q, magnetic multipole M, magnetic toroidal multipole T, and electric toroidal multipole G according to the $\mathcal{P}$ and $\mathcal{T}$ parities in $\boldsymbol{F}$.

From these couplings, one finds what types of multipole degrees of freedom are induced when the external fields and currents are applied under electronic nematic orderings. The different types of multipoles can be induced depending on the types of electric quadrupoles and field direction. For example, when the expectation value of Q_{xy} is nonzero, the rank-1 dipole $\mathcal{D}_y$, the rank-2 quadrupole $\mathcal{Q}_{zx}$, and the rank-3 octupoles $(\mathcal{O}_y^{\alpha}, \mathcal{O}_y^{\beta})$ are induced by the x-directional field F_x, while the rank-2 quadrupole $\mathcal{Q}_v$ and the rank-3 octupole $\mathcal{O}_{xyz}$ are induced by the z-directional field F_z. We summarize the relationship between $\boldsymbol{F}$ and induced multipoles under Q_{2m} in Table 1. We discuss the specific multipoles induced by external fields and currents in the following subsections.

2.2. Electric field

When $\boldsymbol{F}$ corresponds to the electric field $\boldsymbol{E}$ with the spatial inversion and time-reversal parities of $(\mathcal{P}, \mathcal{T}) = (-1, +1)$, $\mathcal{D}$, $\mathcal{Q}$, and $\mathcal{O}$ correspond to the electric dipole Q_{1m}, electric toroidal quadrupole G_{2m}, and electric octupole Q_{3m}, respectively. We discuss several characteristic features by applying $\boldsymbol{E}$.

For the dipole component Q_{1m}, the transverse electric polarization appears for (Q_{yz}, Q_{zx}, Q_{xy}) in addition to the conventional longitudinal one. For example, the $y(x)$-directional electric polarization related to Q_y (Q_x) appears for Q_{xy} under E_x (E_y). It is noted that this transverse response is symmetric by interchanging E_x and E_y, which is in contrast to the antisymmetric rotational response under the ferroaxial ordering; Q_y (Q_x) is induced by E_x (E_y) for the Q_{xy} ordering, while Q_y $(-Q_x)$ is induced by E_x (E_y) for the ferroaxial ordering [71, 72, 73]. Since the electric dipole Q_{1m} leads to the antisymmetric spin splitting in the electronic band structure, the Edelstein effect, where the magnetization is induced by the electric current, can be expected.

Depending on Q_{2m} and $\boldsymbol{E}$, the dipole component vanishes, but the quadrupole component is finite, as shown in Table 1. One of the examples is the situation where E_z is applied to the Q_{xy} state; the electric toroidal quadrupole G_v is induced. This result indicates that the electric field becomes a conjugate field of the electric toroidal quadrupole under the electronic nematic orderings. Thus, physical phenomena brought about by the electric toroidal quadrupole, such as the nonlinear Hall effect based on the Berry curvature dipole mechanism [74] and Edelstein effect discussed in materials hosting the electric toroidal quadrupole [75, 76, 77, 78], are expected.

2.3. Magnetic field

In the case of the magnetic field $\boldsymbol{F} = \boldsymbol{H}$ with $(\mathcal{P}, \mathcal{T}) = (+1, -1)$, the relevant multipoles are rank-1 magnetic dipole M_{1m}, rank-2 magnetic toroidal quadrupole T_{2m}, and rank-3 magnetic octupole M_{3m}. Similarly to the electric field, the transverse magnetization related to the magnetic dipole (M_x, M_y, M_z) is expected for the orderings with (Q_{yz}, Q_{zx}, Q_{xy}). In addition, the magnetic toroidal quadrupole T_{2m} is induced depending on Q_{2m} and $\boldsymbol{H}$. Since the magnetic toroidal quadrupole becomes the origin of the directional-dependent spin current generation arising from the symmetric-type momentum-dependent spin

Table 2: The correspondence between external fields/currents and induced multipoles.

$\boldsymbol{F} = (F_x, F_y, F_z)$	$\mathcal{D}$ (rank 1)	$\mathcal{Q}$ (rank 2)	$\mathcal{O}$ (rank 3)
Electric field $\boldsymbol{E}$	Q_{1m}	G_{2m}	Q_{3m}
Magnetic field $\boldsymbol{H}$	M_{1m}	T_{2m}	M_{3m}
Electric current $\boldsymbol{J}$	T_{1m}	M_{2m}	T_{3m}

splitting in the band structure [79, 80], similar phenomena are also expected when the magnetic field is applied to the electronic nematic orderings. Moreover, the rank-3 magnetic octupole is induced through the coupling between Q_{2m} and $\boldsymbol{H}$, which has been proposed and observed in CeB_6 hosting the electric quadrupole ordered state [81, 82, 83, 84, 85, 86, 87].

2.4. Electric current

Finally, we consider the case of the electric current, i.e., $\boldsymbol{F} = \boldsymbol{J}$. Since the electric current corresponds to the polar vector with time-reversal odd to satisfy $(\mathcal{P}, \mathcal{T}) = (-1, -1)$, the corresponding multipoles to $\mathcal{D}$, $\mathcal{Q}$, and $\mathcal{O}$ are the magnetic toroidal dipole T_{1m}, magnetic quadrupole M_{2m}, and magnetic toroidal octupole T_{3m}, respectively, where the magnetic toroidal dipole becomes the origin of the linear antisymmetric magneto-electric effect [88, 89, 90, 91] and nonreciprocal transport [92, 93], the magnetic quadrupole leads to the linear symmetric magneto-electric effect, current-induced distortion, and nonlinear Hall effect [94, 95, 96, 97, 98, 99, 100], and magnetic toroidal octupole gives rise to nonreciprocal transport owing to the asymmetric band structure [101].

In this way, electronic nematic orderings acquire various functionalities according to the emergence of multipoles when the external fields and currents are applied. We summarize the relationship between external fields/currents and induced multipoles in Table 2. It is noted that the above results can be applied to other vector fields and currents. For example, the spin current in the form of $\boldsymbol{J} \times \boldsymbol{\sigma}$ ($\boldsymbol{\sigma}$ is the spin polarization vector) is categorized into the case of $\boldsymbol{F} = \boldsymbol{E}$. When $\boldsymbol{F}$ corresponds to the time-reversal-even axial vectors, such as the static rotational distortion, the corresponding multipoles are given by the electric toroidal dipole for $\mathcal{D}$, electric quadrupole for $\mathcal{Q}$, and electric toroidal octupole for $\mathcal{O}$.

3. Classification of field-induced multipoles under point group

In this section, we classify the induced multipoles by external fields and currents under magnetic point groups by using the group theory; a similar point-group classification of multipoles in a nematic liquid crystal has also been performed [102, 103]. We here consider five magnetic point groups, $4/mmm1'$, $6/mmm1'$, $\bar{3}m1'$, $mmm1'$, and $2/m1'$, where any of electric quadrupoles Q_{2m} belong to the totally symmetric irreducible representation; the results for other

Table 3: Multipoles induced by the electric field $\boldsymbol{E} = (E_x, E_y, E_z)$, the magnetic field $\boldsymbol{H} = (H_x, H_y, H_z)$, and the electric current $\boldsymbol{J} = (J_x, J_y, J_z)$ under the tetragonal magnetic point group (MPG) $4/mmm1'$. We omit the multipoles for the electric monopole and the electric toroidal octupole for simplicity.

$\boldsymbol{F}$	MPG	multipoles
—	$4/mmm1'$	Q_u
E_x	$2mm1'$	Q_x, Q_v, Q_x^α, Q_x^β, G_{yz}
E_y	$m2m1'$	Q_y, Q_v, Q_y^α, Q_y^β, G_{zx}
E_z	$4mm1'$	Q_z, Q_z^α
H_x	$mm'm'$	Q_v, M_x, M_x^α, M_x^β, T_{yz}
H_y	$m'mm'$	Q_v, M_y, M_y^α, M_y^β, T_{zx}
H_z	$4/mm'm'$	M_z, M_z^α
J_x	$m'mm$	Q_v, T_x, T_x^α, T_x^β, M_{yz}
J_y	$mm'm$	Q_v, T_y, T_y^α, T_y^β, M_{zx}
J_z	$4/m'mm$	T_z, T_z^α

Table 4: Multipoles induced by $\boldsymbol{E} = (E_x, E_y, E_z)$, $\boldsymbol{H} = (H_x, H_y, H_z)$, and $\boldsymbol{J} = (J_x, J_y, J_z)$ under the hexagonal magnetic point group (MPG) $6/mmm1'$. We omit the multipoles for the electric monopole and the electric toroidal octupole for simplicity.

$\boldsymbol{F}$	MPG	multipoles
—	$6/mmm1'$	Q_u
E_x	$2mm1'$	Q_x, Q_v, Q_x^α, Q_x^β, G_{yz}
E_y	$m2m1'$	Q_y, Q_v, Q_y^α, Q_y^β, G_{zx}
E_z	$6mm1'$	Q_z, Q_z^α
H_x	$mm'm'$	Q_v, M_x, M_x^α, M_x^β, T_{yz}
H_y	$m'mm'$	Q_v, M_y, M_y^α, M_y^β, T_{zx}
H_z	$6/mm'm'$	M_z, M_z^α
J_x	$m'mm$	Q_v, T_x, T_x^α, T_x^β, M_{yz}
J_y	$mm'm$	Q_v, T_y, T_y^α, T_y^β, M_{zx}
J_z	$6/m'mm$	T_z, T_z^α

magnetic point groups can be straightforwardly obtained by using the compatible relations between the above groups and subgroups [104]. In each point group, we show the symmetry reduction by the electric field $\boldsymbol{E} = (E_x, E_y, E_z)$, the magnetic field $\boldsymbol{H} = (H_x, H_y, H_z)$, and the electric current $\boldsymbol{J} = (J_x, J_y, J_z)$, and present the induced multipoles. The notations of the crystal axes and the multipoles are followed by Ref. [104]. We show the results for the tetragonal magnetic point group $4/mmm1'$ in Table 3, the hexagonal magnetic point group $6/mmm1'$ in Table 4, the trigonal magnetic point group $\bar{3}m1'$ in Table 5, the orthorhombic magnetic point group $mmm1'$ in Table 6, and the monoclinic

Table 5: Multipoles induced by $\boldsymbol{E}=(E_x,E_y,E_z)$, $\boldsymbol{H}=(H_x,H_y,H_z)$, and $\boldsymbol{J}=(J_x,J_y,J_z)$ under the trigonal magnetic point group (MPG) $\bar{3}m1'$. We omit the multipoles for the electric monopole, the electric toroidal dipole, and the electric toroidal octupole for simplicity.

$\boldsymbol{F}$	MPG	multipoles
—	$\bar{3}m1'$	Q_u
E_x	$m1'$	Q_x, Q_z, Q_v, Q_{zx}, Q_x^α, Q_z^α, Q_x^β, Q_z^β, G_{yz}, G_{xy}
E_y	$21'$	Q_y, Q_v, Q_{zx}, Q_{xyz}, Q_y^α, Q_y^β, G_0, G_u, G_v, G_{zx}
E_z	$3m1'$	Q_z, Q_z^α, Q_{3a}
H_x	$2'/m'$	Q_v, Q_{zx}, M_x, M_z, M_x^α, M_z^α, M_x^β, M_z^β, T_{yz}, T_{xy}
H_y	$2/m$	Q_v, Q_{zx}, M_y, M_{xyz}, M_y^α, M_y^β, T_0, T_u, T_v, T_{zx}
H_z	$\bar{3}m'$	M_z, M_z^α, M_{3a}
J_x	$2'/m$	Q_v, Q_{zx}, T_x, T_z, T_x^α, T_z^α, T_x^β, T_z^β, M_{yz}, M_{xy}
J_y	$2/m'$	Q_v, Q_{zx}, T_y, T_{xyz}, T_y^α, T_y^β, M_0, M_u, M_v, M_{zx}
J_z	$\bar{3}'m$	T_z, T_z^α, T_{3a}

Table 6: Multipoles induced by $\boldsymbol{E}=(E_x,E_y,E_z)$, $\boldsymbol{H}=(H_x,H_y,H_z)$, and $\boldsymbol{J}=(J_x,J_y,J_z)$ under the orthorhombic magnetic point group (MPG) $mmm1'$. We omit the multipoles for the electric monopole and the electric toroidal octupole for simplicity.

$\boldsymbol{F}$	MPG	multipoles
—	$mmm1'$	Q_u, Q_v
E_x	$2mm1'$	Q_x, Q_x^α, Q_x^β, G_{yz}
E_y	$m2m1'$	Q_y, Q_y^α, Q_y^β, G_{zx}
E_z	$mm21'$	Q_z, Q_z^α, Q_z^β, G_{xy}
H_x	$mm'm'$	M_x, M_x^α, M_x^β, T_{yz}
H_y	$m'mm'$	M_y, M_y^α, M_y^β, T_{zx}
H_z	$m'm'm$	M_z, M_z^α, M_z^β, T_{xy}
J_x	$m'mm$	T_x, T_x^α, T_x^β, M_{yz}
J_y	$mm'm$	T_y, T_y^α, T_y^β, M_{zx}
J_z	mmm'	T_z, T_z^α, T_z^β, M_{xy}

magnetic point group $2/m1'$ in Table 7.

We discuss the result for $4/mmm1'$ in Table 3, where the electric quadrupole Q_u belongs to the totally symmetric irreducible representation. When the x-directional electric field E_x is applied, the electric dipole Q_x, the electric quadrupole Q_v, the electric octupoles (Q_x^α, Q_x^β), and the electric toroidal quadrupole G_{yz} are induced. Among them, $(Q_x, G_{yz}, Q_x^\alpha, Q_y^\alpha)$ results from the coupling between Q_u and E_x, as shown in Table 1. Meanwhile, the remaining Q_v is secondary induced through the symmetry lowering by the breaking of the four-fold rotational symmetry. When the x-directional magnetic field H_x is applied, the multipoles with opposite $\mathcal{P}$ and $\mathcal{T}$ parities, $(M_x, T_{yz}, M_x^\alpha, M_x^\beta)$, are induced except for Q_v. Similarly, the x-directional electric current J_x induces the multipoles with the opposite $\mathcal{T}$ parity, $(T_x, M_{yz}, T_x^\alpha, T_x^\beta)$, are induced except for Q_v.

Table 7: Multipoles induced by $\boldsymbol{E} = (E_x, E_y, E_z)$, $\boldsymbol{H} = (H_x, H_y, H_z)$, and $\boldsymbol{J} = (J_x, J_y, J_z)$ under the monoclinic magnetic point group (MPG) $2/m1'$. We omit the multipoles for the electric monopole, the electric toroidal dipole, and the electric toroidal octupole for simplicity.

$\boldsymbol{F}$	MPG	multipoles
—	$2/m1'$	Q_u, Q_v, Q_{zx}
E_x, E_z	$m1'$	Q_x, Q_z, Q_x^α, Q_z^α, Q_x^β, Q_z^β, G_{yz}, G_{xy}
E_y	$21'$	Q_y, Q_{xyz}, Q_y^α, Q_y^β, G_0, G_u, G_v, G_{zx}
H_x, H_z	$2'/m'$	M_x, M_z, M_x^α, M_z^α, M_x^β, M_z^β, T_{yz}, T_{xy}
H_y	$2/m$	M_y, M_{xyz}, M_y^α, M_y^β, T_0, T_u, T_v, T_{zx}
J_x, J_z	$2'/m$	T_x, T_z, T_x^α, T_z^α, T_x^β, T_z^β, M_{yz}, M_{xy}
J_y	$2/m'$	T_y, T_{xyz}, T_y^α, T_y^β, M_0, M_u, M_v, M_{zx}

These results are consistent with the results in Sect. 2. In this way, Eqs. (1)–(15) provide useful information to deduce the multipoles by external fields and currents under the electronic nematic orderings with the electric quadrupole.

4. Multipole couplings in atomic model

In this section, we briefly discuss the symmetry-allowed multipole couplings induced by external fields in Sect. 2 by using an atomic model. We consider the single-site atomic Hamiltonian under the point group $mmm1'$, which is given by

$$\mathcal{H} = -\Delta Q_v - \boldsymbol{h}^{(\mathrm{E})} \cdot \boldsymbol{Q} - \boldsymbol{h}^{(\mathrm{M})} \cdot \boldsymbol{M}, \tag{16}$$

where the first term represents the effect of the crystalline electric field under $mmm1'$; we ignore the effect of Q_u for simplicity. The second term represents the effect of the external electric field with $\boldsymbol{h}^{(\mathrm{E})} = (h_x^{(\mathrm{E})}, h_y^{(\mathrm{E})}, 0)$, where we mimic such an effect as the coupling to the electric dipole $\boldsymbol{Q}$. The third term represents the effect of the external magnetic field $\boldsymbol{h}^{(\mathrm{M})} = (h_x^{(\mathrm{M})}, h_y^{(\mathrm{M})}, 0)$, which couples to the magnetic dipole $\boldsymbol{M}$.

First, we consider the effect of the electric field by setting $\boldsymbol{h}^{(\mathrm{M})} = \boldsymbol{0}$. We consider the p–d orbital system so that the electric dipole (Q_x, Q_y) and the electric toroidal quadrupole (G_{yz}, G_{zx}) are included in the physical Hilbert space. The matrix elements for these multipoles as well as the electric quadrupole Q_v are given by

$$Q_v = \frac{1}{35}\begin{pmatrix} 7\sqrt{3} & 0 & 0 & 0 & 0 & 0 & 0 & 0 \\ 0 & -7\sqrt{3} & 0 & 0 & 0 & 0 & 0 & 0 \\ 0 & 0 & 0 & 0 & 0 & 0 & 0 & 0 \\ 0 & 0 & 0 & 0 & -10 & 0 & 0 & 0 \\ 0 & 0 & 0 & -10 & 0 & 0 & 0 & 0 \\ 0 & 0 & 0 & 0 & 0 & -5\sqrt{3} & 0 & 0 \\ 0 & 0 & 0 & 0 & 0 & 0 & 5\sqrt{3} & 0 \\ 0 & 0 & 0 & 0 & 0 & 0 & 0 & 0 \end{pmatrix},$$

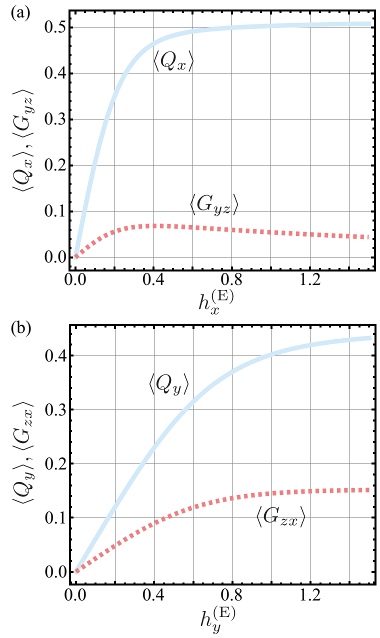

Figure 2: Electric field dependence of electric dipoles (Q_x, Q_y) and electric toroidal quadrupoles (G_{yz}, G_{zx}) in the model in Eq. (16) for $\boldsymbol{h}^{(\mathrm{M})} = \mathbf{0}$ and $\Delta = 1$. The field direction is taken along the x direction in (a) and the y direction in (b).

$$Q_x = \frac{1}{\sqrt{15}} \begin{pmatrix} 0 & 0 & 0 & -1 & \sqrt{3} & 0 & 0 & 0 \\ 0 & 0 & 0 & 0 & 0 & 0 & 0 & \sqrt{3} \\ 0 & 0 & 0 & 0 & 0 & 0 & \sqrt{3} & 0 \\ -1 & 0 & 0 & 0 & 0 & 0 & 0 & 0 \\ \sqrt{3} & 0 & 0 & 0 & 0 & 0 & 0 & 0 \\ 0 & 0 & 0 & 0 & 0 & 0 & 0 & 0 \\ 0 & 0 & \sqrt{3} & 0 & 0 & 0 & 0 & 0 \\ 0 & \sqrt{3} & 0 & 0 & 0 & 0 & 0 & 0 \end{pmatrix},$$

$$Q_y = \frac{1}{\sqrt{15}} \begin{pmatrix} 0 & 0 & 0 & 0 & 0 & 0 & 0 & \sqrt{3} \\ 0 & 0 & 0 & -1 & -\sqrt{3} & 0 & 0 & 0 \\ 0 & 0 & 0 & 0 & 0 & \sqrt{3} & 0 & 0 \\ 0 & -1 & 0 & 0 & 0 & 0 & 0 & 0 \\ 0 & -\sqrt{3} & 0 & 0 & 0 & 0 & 0 & 0 \\ 0 & 0 & \sqrt{3} & 0 & 0 & 0 & 0 & 0 \\ 0 & 0 & 0 & 0 & 0 & 0 & 0 & 0 \\ \sqrt{3} & 0 & 0 & 0 & 0 & 0 & 0 & 0 \end{pmatrix},$$

$$
G_{yz} = \frac{2}{3\sqrt{15}} \begin{pmatrix} 0 & 0 & 0 & -\sqrt{3} & -1 & 0 & 0 & 0 \\ 0 & 0 & 0 & 0 & 0 & 0 & 0 & -1 \\ 0 & 0 & 0 & 0 & 0 & 0 & 1 & 0 \\ -\sqrt{3} & 0 & 0 & 0 & 0 & 0 & 0 & 0 \\ -1 & 0 & 0 & 0 & 0 & 0 & 0 & 0 \\ 0 & 0 & 0 & 0 & 0 & 0 & 0 & 0 \\ 0 & 0 & 1 & 0 & 0 & 0 & 0 & 0 \\ 0 & -1 & 0 & 0 & 0 & 0 & 0 & 0 \end{pmatrix},
$$

$$
G_{zx} = \frac{2}{3\sqrt{15}} \begin{pmatrix} 0 & 0 & 0 & 0 & 0 & 0 & 0 & 1 \\ 0 & 0 & 0 & \sqrt{3} & -1 & 0 & 0 & 0 \\ 0 & 0 & 0 & 0 & 0 & -1 & 0 & 0 \\ 0 & \sqrt{3} & 0 & 0 & 0 & 0 & 0 & 0 \\ 0 & -1 & 0 & 0 & 0 & 0 & 0 & 0 \\ 0 & 0 & -1 & 0 & 0 & 0 & 0 & 0 \\ 0 & 0 & 0 & 0 & 0 & 0 & 0 & 0 \\ 1 & 0 & 0 & 0 & 0 & 0 & 0 & 0 \end{pmatrix}, \qquad (17)
$$

where the basis is represented by $\{\phi_x, \phi_y, \phi_z, \phi_u, \phi_v, \phi_{yz}, \phi_{zx}, \phi_{xy}\}$; (ϕ_x, ϕ_y, ϕ_z) denotes the three p-orbital wave functions and $(\phi_u, \phi_v, \phi_{yz}, \phi_{zx}, \phi_{xy})$ denotes the five d-orbital wave functions. The subscript u and v stand for $3z^2 - r^2$ and $x^2 - y^2$, respectively.

We show the expectation values of the electric dipole Q_x and the electric toroidal quadrupole G_{yz}, $\langle Q_x \rangle$ and $\langle G_{yz} \rangle$, against $h_x^{(\mathrm{E})}$ in Fig. 2(a). We set $\Delta = 1$, $h_y^{(\mathrm{E})} = 0$, and the temperature $T = 0.1$. One finds that $\langle G_{yz} \rangle$ becomes nonzero for $h_x^{(\mathrm{E})} \neq 0$, which indicates that the external electric field induces the electric toroidal quadrupole, as expected from the symmetry argument in Sect. 2 [105]. We also show the results under the y-directional electric field in Fig. 2(b) by setting $h_x^{(\mathrm{E})} = 0$ and $h_y^{(\mathrm{E})} \neq 0$, where $\langle Q_y \rangle$ and $\langle G_{zx} \rangle$ are induced instead of $\langle Q_x \rangle$ and $\langle G_{yz} \rangle$. The different values of $\langle Q_x \rangle$ and $\langle Q_y \rangle$ are attributed to the fourfold symmetry breaking under the orthorhombic crystalline electric field Q_v. Indeed, we confirm that $\langle Q_x \rangle$ under $h_x^{(\mathrm{E})}$ is equal to $\langle Q_y \rangle$ under $h_y^{(\mathrm{E})}$ when $\Delta = 0$.

Next, we consider the effect of the magnetic field by setting $\boldsymbol{h}^{(\mathrm{E})} = \mathbf{0}$. We consider the s–d orbital system, where the relevant multipole matrix elements in the following calculations are given by

$$
Q_v = \frac{1}{7\sqrt{5}} \begin{pmatrix} 0 & 0 & 7 & 0 & 0 & 0 \\ 0 & 0 & -2\sqrt{5} & 0 & 0 & 0 \\ 7 & -2\sqrt{5} & 0 & 0 & 0 & 0 \\ 0 & 0 & 0 & -\sqrt{15} & 0 & 0 \\ 0 & 0 & 0 & 0 & \sqrt{15} & 0 \\ 0 & 0 & 0 & 0 & 0 & 0 \end{pmatrix},
$$

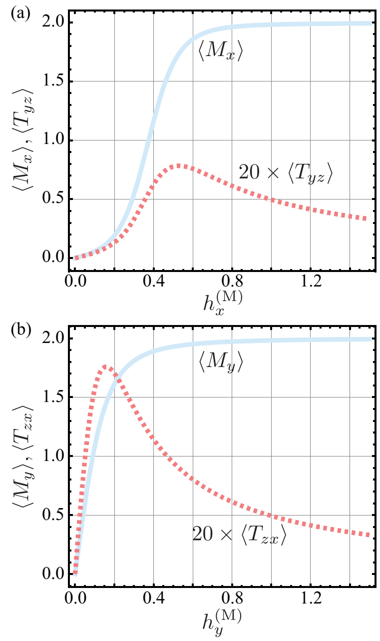

Figure 3: Magnetic field dependence of magnetic dipoles (M_x, M_y) and magnetic toroidal quadrupoles (T_{yz}, T_{zx}) in the model in Eq. (16) for $\boldsymbol{h}^{(\mathrm{E})} = \boldsymbol{0}$ and $\Delta = 1$. The field direction is taken along the x direction in (a) and the y direction in (b).

$$M_x = \begin{pmatrix} 0 & 0 & 0 & 0 & 0 & 0 \\ 0 & 0 & 0 & i\sqrt{3} & 0 & 0 \\ 0 & 0 & 0 & i & 0 & 0 \\ 0 & -i\sqrt{3} & -i & 0 & 0 & 0 \\ 0 & 0 & 0 & 0 & 0 & i \\ 0 & 0 & 0 & 0 & -i & 0 \end{pmatrix},$$

$$M_y = \begin{pmatrix} 0 & 0 & 0 & 0 & 0 & 0 \\ 0 & 0 & 0 & 0 & -i\sqrt{3} & 0 \\ 0 & 0 & 0 & 0 & i & 0 \\ 0 & 0 & 0 & 0 & 0 & -i \\ 0 & i\sqrt{3} & -i & 0 & 0 & 0 \\ 0 & 0 & 0 & i & 0 & 0 \end{pmatrix},$$

$$T_{yz} = \frac{1}{2\sqrt{5}} \begin{pmatrix} 0 & 0 & 0 & i & 0 & 0 \\ 0 & 0 & 0 & 0 & 0 & 0 \\ 0 & 0 & 0 & 0 & 0 & 0 \\ -i & 0 & 0 & 0 & 0 & 0 \\ 0 & 0 & 0 & 0 & 0 & 0 \\ 0 & 0 & 0 & 0 & 0 & 0 \end{pmatrix},$$

$$T_{zx} = \frac{1}{2\sqrt{5}} \begin{pmatrix} 0 & 0 & 0 & 0 & i & 0 \\ 0 & 0 & 0 & 0 & 0 & 0 \\ 0 & 0 & 0 & 0 & 0 & 0 \\ 0 & 0 & 0 & 0 & 0 & 0 \\ -i & 0 & 0 & 0 & 0 & 0 \\ 0 & 0 & 0 & 0 & 0 & 0 \end{pmatrix}, \tag{18}$$

where the basis is represented by $\{\phi_s, \phi_u, \phi_v, \phi_{yz}, \phi_{zx}, \phi_{xy}\}$; ϕ_s represents the s-orbital wave function.

Figure 3(a) shows the x-directional magnetic field dependence of expectation values of the magnetic dipole M_x and magnetic toroidal quadrupole T_{yz} for $\Delta = 1$, $h_y^{(\mathrm{M})} = 0$, and $T = 0.1$. The magnetic toroidal quadrupole $\langle T_{yz} \rangle$ becomes nonzero for $h_x^{(\mathrm{M})} \neq 0$ as expected from the symmetry argument in Sect. 2.1 [105]. Furthermore, one finds that a different component of magnetic toroidal quadrupole, T_{zx}, is induced when the magnetic field direction changes from the x direction to the y direction, as shown in Fig. 3(b). Similarly to the case of the electric field, the behaviors of M_x and M_y are different from each other owing to the lack of fourfold rotational symmetry under Q_v. In this way, the coupling between the magnetic field and magnetic toroidal quadrupole occurs in the microscopic model when the orbital degrees of freedom are taken into account.

Let us comment on a candidate system to realize such a situation. Since both electric toroidal quadrupole and magnetic toroidal quadrupole are active in the hybridized-orbital space, the situation with a small energy splitting between p and d or s and d orbitals is desirable. This indicates that the materials containing heavier elements with a smaller energy difference are candidate materials. On the other hand, the above electric toroidal quadrupole and magnetic toroidal quadrupole are also activated by other degrees of freedom in solids. For example, a particular type of bond modulation is related to the electric toroidal quadrupole as found in $Cd_2Re_2O_7$ [106, 76, 107, 108] and that of antiferromagnetic structure is related to the magnetic toroidal quadrupole as found in CoF_2 [109, 79]. Thus, one has a possibility of searching for the emergence of these active multipoles through not only the atomic-scale but also cluster electronic degrees of freedom.

5. Spin splitting under external fields

Although the direct observation of the higher-order and/or toroidal-type multipoles under external fields and currents is often difficult in experiments, one can find the appearance of these multipoles by looking into electronic band structures and physical phenomena. In order to demonstrate that, we consider a fundamental tight-binding model consisting of the s and two (p_x, p_y) orbitals on a two-dimensional square lattice (the lattice constant is set as unity), which is given by

$$\mathcal{H} = \sum_{\boldsymbol{k}\nu\nu'\sigma\sigma'} c^{\dagger}_{\boldsymbol{k}\nu\sigma} [\delta_{\sigma\sigma'} H_\sigma(\boldsymbol{k}) + \delta_{\sigma\sigma'} h_v H_v - \delta_{\sigma\sigma'} H H_M^z - E H_E^z]^{\nu\nu'}_{\sigma\sigma'} c_{\boldsymbol{k}\nu'\sigma'}, \tag{19}$$

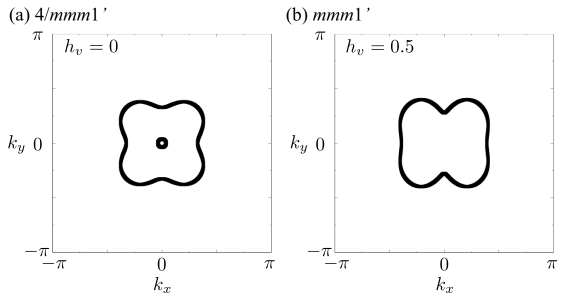

Figure 4: Isoenergy surfaces under (a) the $4/mmm1'$ symmetry for $h_v = 0$ and (b) the $mmm1'$ symmetry for $h_v = 0.5$ at the chemical potential $\mu = 3.3$. The other model parameters are $t_\sigma = 1$, $t_\pi = 0.5$, $t_{xy} = 0.3$, $t_s = 0.8$, $t_{sp} = 0.6$, and $\lambda = 0.2$.

where $c^\dagger_{\boldsymbol{k}\nu\sigma}$ and $c_{\boldsymbol{k}\nu\sigma}$ are creation and annihilation operators at wave vector $\boldsymbol{k}$, orbital $\nu = s, p_x, p_y$, and spin σ, respectively. The 3×3 matrix $H_\sigma(\boldsymbol{k})$ appearing in the first term in Eq. (19) is represented by

$$H_\sigma(\boldsymbol{k}) = \left(\begin{array}{ccc} 2t_s(\cos k_x + \cos k_y) & -2it_{sp}\sin k_x & -2it_{sp}\sin k_y \\ 2it_{sp}\sin k_x & 2(t_\sigma \cos k_x + t_\pi \cos k_y) & 2t_{xy}\sin k_x \sin k_y - i\sigma\lambda \\ 2it_{sp}\sin k_y & 2t_{xy}\sin k_x \sin k_y + i\sigma\lambda & 2(t_\sigma \cos k_y + t_\pi \cos k_x) \end{array} \right), \tag{20}$$

where the basis is given by $(\phi_{s\sigma}, \phi_{x\sigma}, \phi_{y\sigma})$, which denotes the s-, p_x-, and p_y-orbital wave functions with the spin degree of freedom σ, respectively. t_s, t_{sp}, (t_σ, t_π), t_{xy}, and λ represent the hopping between s orbitals, hopping between s and (p_x, p_y) orbitals, hopping between p_x or p_y orbitals, hopping between p_x and p_y orbitals, and atomic spin–orbit coupling, respectively. We omit the atomic energy term for s and p orbitals, since it does not affect the following result. The second term in Eq. (19) represents the symmetry-lowering crystalline electric field to the $mmm1'$ symmetry, which split the energy levels in terms of the p_x and p_y orbitals. The matrix H_v is given by

$$H_v = \left(\begin{array}{ccc} 0 & 0 & 0 \\ 0 & 1 & 0 \\ 0 & 0 & -1 \end{array} \right). \tag{21}$$

It is noted that the symmetry of the model corresponds to $4/mmm1'$ for $h_v = 0$ and $mmm1'$ for $h_v \neq 0$. The third term in Eq. (19) represents the effect of the magnetic field along the z direction. We consider the Zeeman coupling for the s orbital without loss of generality, whose Hamiltonian matrix H^z_M is given by

$$H^z_M = \left(\begin{array}{ccc} \sigma & 0 & 0 \\ 0 & 0 & 0 \\ 0 & 0 & 0 \end{array} \right). \tag{22}$$

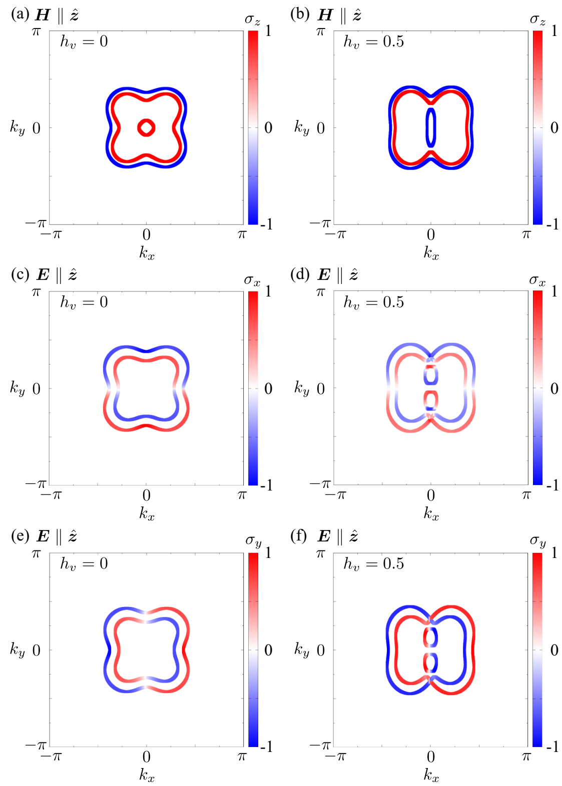

Figure 5: Isoenergy surfaces under (a, c, e) the $4/mmm1'$ symmetry for $h_v = 0$ and (b, d, f) the $mmm1'$ symmetry for $h_v = 0.5$ at the chemical potential $\mu = 3.3$. The results in (a, b) show the symmetric spin splitting induced by the magnetic field $H = 0.2$, while those in (c, d, e, f) show the antisymmetric spin splitting induced by the electric field $E = 0.2$. The other model parameters are $t_\sigma = 1$, $t_\pi = 0.5$, $t_{xy} = 0.3$, $t_s = 0.8$, $t_{sp} = 0.6$, and $\lambda = 0.2$. The color map shows the spin polarization of (a, b) the z, (c, d) x, and (e, f) y components at each wave vector.

The fourth term in Eq. (19) represents the effect of the electric field along the z direction. We mimic the effect of the electric field as the coupling to the electric dipole degree of freedom in the system for simplicity, which is included in the s-p-orbital space as a spin-dependent form [110]. The matrix H_E^z is given by

$$H_E^z = \begin{pmatrix} 0 & 0 & 0 & 0 & 1 & -i \\ 0 & 0 & 0 & -1 & 0 & 0 \\ 0 & 0 & 0 & i & 0 & 0 \\ 0 & -1 & -i & 0 & 0 & 0 \\ 1 & 0 & 0 & 0 & 0 & 0 \\ i & 0 & 0 & 0 & 0 & 0 \end{pmatrix}, \tag{23}$$

where the basis is given by $(\phi_{s\uparrow}, \phi_{x\uparrow}, \phi_{y\uparrow}, \phi_{s\downarrow}, \phi_{x\downarrow}, \phi_{y\downarrow})$.

Figure 4(a) shows the isoenergy surfaces under the $4/mmm1'$, i.e., $h_v = 0$. The other model parameters are set as $t_\sigma = 1$, $t_\pi = 0.5$, $t_{xy} = 0.3$, $t_s = 0.8$, $t_{sp} = 0.6$, $\lambda = 0.2$, $H = 0$, and $E = 0$. The isoenergy surfaces are fourfold symmetric owing to the tetragonal symmetry. When the effect of the orthorhombic distortion is introduced by taking $h_v \neq 0$, the symmetry of the system is lowered into $mmm1'$; the isoenergy surfaces are deformed so as to break the fourfold rotational symmetry, as shown in Fig. 4(b).

We show the change of the isoenergy surfaces when either the magnetic field H or the electric field E is applied in Fig. 5. Both results in Figs. 5(a) and 5(b) in the presence of H exhibit the symmetric spin splitting in terms of the z-spin component in the isoenergy surface, although their functional forms are different from each other. In the case of $4/mmm1'$ in Fig. 5(a), the symmetric spin splitting is fourfold-symmetric, while it is twofold-symmetric in the case of $mmm1'$ in Fig. 5(b). Especially, one finds that the small isoenergy surface with the negative z-spin polarization around $\boldsymbol{k} = (0, 0)$ is elongated along the y direction in Fig. 5(b), which means that an additional component from the Zeeman splitting inducing the uniform spin splitting happens. Indeed, such a symmetric spin splitting is understood by considering the emergence of the magnetic toroidal quadrupole T_{xy}, which becomes the origin of the symmetric spin splitting in the form of $-(k_x^2 - k_y^2)\sigma_x$ for $k_z = 0$ [65]; the result is consistent with the symmetry analysis in Table 6. Thus, the application of the magnetic field to the electronic nematic ordering leads to unconventional symmetric spin splitting, which can be an indirect probe of the magnetic toroidal quadrupole.

Next, we discuss the result when the electric field E is applied. As shown in Figs. 5(c) and 5(e), the Rashba-type antisymmetric spin splitting in the form of $k_x\sigma_y - k_y\sigma_x$ is found under the $4/mmm1'$ symmetry. This is attributed to the activation of the electric dipole degree of freedom, which is directly coupled to the electric field. On the other hand, one finds an additional antisymmetric spin splitting in the case of the $mmm1'$ symmetry according to the inequivalence between k_x and k_y directions, as shown in Figs. 5(d) and 5(f), which indicates the contribution from the electric toroidal quadrupole G_{xy} with the functional form of $k_x\sigma_y + k_y\sigma_x$. This is also consistent with the symmetry analysis in Table 6. Thus, the emergence of the electric toroidal quadrupole can be detected by looking into the antisymmetric spin-split band structure in spin- and angle-resolved photoemission spectroscopy.

6. Summary

We have investigated the nature of the electronic nematic orderings by focusing on the effect of external fields and currents accompanying the breakings of the spatial inversion and/or time-reversal symmetries. Based on the multipole representation consisting of four-type multipoles, we showed the conditions to activate rank-1 dipole, rank-2 quadrupole, and rank-3 octupole moments with distinct spatial inversion and time-reversal parities. In contrast to the conventional isotropic system, the nematic states characterized by the electric quadrupole exhibit peculiar responses to external stimuli according to the induced unconventional multipoles; the electric toroidal quadrupole, the magnetic toroidal quadrupole, and the magnetic quadrupole are induced by the electric field, magnetic field, and electric current. We also summarized the classification of multipoles under several magnetic point groups in a systematic way. We demonstrate the emergence of unconventional multipole moments in external fields by analyzing the atomic multi-orbital model. Moreover, we show that the effect of the field-induced multipoles can be detected by the spin-split band structure. Our results provide further exploration of characteristic physical phenomena under electronic nematic orderings by external fields and currents.

This research was supported by JSPS KAKENHI Grants Numbers JP21H01037, JP22H04468, JP22H00101, JP22H01183, JP23H04869, JP23K03288, and by JST PRESTO (JPMJPR20L8) and JST CREST (JPMJCR23O4).

References

[1] Y. Tokura, N. Nagaosa, Orbital physics in transition-metal oxides, Science 288 (5465) (2000) 462–468.

[2] S. V. Streltsov, D. I. Khomskii, Orbital physics in transition metal compounds: new trends, Phys. Usp. 60 (11) (2017) 1121.

[3] D. I. Khomskii, S. V. Streltsov, Orbital effects in solids: Basics, recent progress, and opportunities, Chem. Rev. 121 (5) (2021) 2992–3030.

[4] E. Fradkin, S. A. Kivelson, M. J. Lawler, J. P. Eisenstein, A. P. Mackenzie, Nematic Fermi fluids in condensed matter physics, Annu. Rev. Condens. Matter Phys. 1 (1) (2010) 153–178.

[5] R. Fernandes, A. Chubukov, J. Schmalian, What drives nematic order in iron-based superconductors?, Nat. Phys. 10 (2) (2014) 97–104.

[6] I. Pomeranchuk, Sov. phys. jetp 8, 361 (1959), Sov. Phys. JETP 8 (1959) 361.

[7] H. Yamase, H. Kohno, Possible quasi-one-dimensional Fermi surface in $La_{2-x}Sr_xCuO_4$, J. Phys. Soc. Jpn. 69 (2) (2000) 332–335. doi:10.1143/JPSJ.69.332.

[8] C. J. Halboth, W. Metzner, d-wave superconductivity and pomeranchuk instability in the two-dimensional Hubbard model, Phys. Rev. Lett. 85 (2000) 5162–5165. doi:10.1103/PhysRevLett.85.5162.

[9] G. Fáth, J. Sólyom, Search for the nondimerized quantum nematic phase in the spin-1 chain, Phys. Rev. B 51 (1995) 3620–3625. doi:10.1103/PhysRevB.51.3620.

[10] A. Läuchli, G. Schmid, S. Trebst, Spin nematics correlations in bilinear-biquadratic $s = 1$ spin chains, Phys. Rev. B 74 (2006) 144426. doi:10.1103/PhysRevB.74.144426.

[11] S. R. Manmana, A. M. Läuchli, F. H. L. Essler, F. Mila, Phase diagram and continuous pair-unbinding transition of the bilinear-biquadratic $s = 1$ Heisenberg chain in a magnetic field, Phys. Rev. B 83 (2011) 184433. doi:10.1103/PhysRevB.83.184433.

[12] H. Tsunetsugu, M. Arikawa, Spin nematic phase in s= 1 triangular antiferromagnets, J. Phys. Soc. Jpn. 75 (8) (2006) 083701–083701. doi:10.1143/JPSJ.75.083701.

[13] N. Shannon, T. Momoi, P. Sindzingre, Nematic order in square lattice frustrated ferromagnets, Phys. Rev. Lett. 96 (2006) 027213. doi:10.1103/PhysRevLett.96.027213.

[14] R. Shindou, T. Momoi, $SU(2)$ slave-boson formulation of spin nematic states in $s = \frac{1}{2}$ frustrated ferromagnets, Phys. Rev. B 80 (2009) 064410. doi:10.1103/PhysRevB.80.064410.

[15] H. Tsunetsugu, M. Arikawa, The spin nematic state in triangular antiferromagnets, J. Phys.: Condens. Matter 19 (14) (2007) 145248. doi:10.1088/0953-8984/19/14/145248.

[16] A. Smerald, N. Shannon, Theory of spin excitations in a quantum spin-nematic state, Phys. Rev. B 88 (2013) 184430. doi:10.1103/PhysRevB.88.184430.

[17] S. A. Kivelson, E. Fradkin, V. J. Emery, Electronic liquid-crystal phases of a doped mott insulator, Nature 393 (6685) (1998) 550–553.

[18] E. Fradkin, S. A. Kivelson, Liquid-crystal phases of quantum Hall systems, Phys. Rev. B 59 (1999) 8065–8072. doi:10.1103/PhysRevB.59.8065.

[19] V. J. Emery, E. Fradkin, S. A. Kivelson, T. C. Lubensky, Quantum theory of the smectic metal state in stripe phases, Phys. Rev. Lett. 85 (2000) 2160–2163. doi:10.1103/PhysRevLett.85.2160.

[20] H.-Y. Kee, Y. B. Kim, Itinerant metamagnetism induced by electronic nematic order, Phys. Rev. B 71 (2005) 184402. doi:10.1103/PhysRevB.71.184402.

[21] T.-M. Chuang, M. Allan, J. Lee, Y. Xie, N. Ni, S. L. Bud'ko, G. Boebinger, P. Canfield, J. Davis, Nematic electronic structure in the "parent" state of the iron-based superconductor $Ca(Fe_{1-x}Co_x)_2As_2$, Science 327 (5962) (2010) 181–184. doi:10.1126/science.1181083.

[22] T. Goto, R. Kurihara, K. Araki, K. Mitsumoto, M. Akatsu, Y. Nemoto, S. Tatematsu, M. Sato, Quadrupole effects of layered iron pnictide superconductor $Ba(Fe_{0.9}Co_{0.1})_2As_2$, J. Phys. Soc. Jpn. 80 (7) (2011) 073702. doi:10.1143/JPSJ.80.073702.

[23] M. Yoshizawa, D. Kimura, T. Chiba, S. Simayi, Y. Nakanishi, K. Kihou, C.-H. Lee, A. Iyo, H. Eisaki, M. Nakajima, S.-i. Uchida, Structural quantum criticality and superconductivity in iron-based superconductor $Ba(Fe_{1-x}Co_x)_2As_2$, J. Phys. Soc. Jpn. 81 (2) (2012) 024604. doi:10.1143/JPSJ.81.024604.

[24] C. Fang, H. Yao, W.-F. Tsai, J. Hu, S. A. Kivelson, Theory of electron nematic order in LaFeAsO, Phys. Rev. B 77 (2008) 224509. doi:10.1103/PhysRevB.77.224509.

[25] R. M. Fernandes, L. H. VanBebber, S. Bhattacharya, P. Chandra, V. Keppens, D. Mandrus, M. A. McGuire, B. C. Sales, A. S. Sefat, J. Schmalian, Effects of nematic fluctuations on the elastic properties of iron arsenide superconductors, Phys. Rev. Lett. 105 (2010) 157003. doi:10.1103/PhysRevLett.105.157003.

[26] F. Krüger, S. Kumar, J. Zaanen, J. van den Brink, Spin-orbital frustrations and anomalous metallic state in iron-pnictide superconductors, Phys. Rev. B 79 (2009) 054504. doi:10.1103/PhysRevB.79.054504.

[27] W. Lv, J. Wu, P. Phillips, Orbital ordering induces structural phase transition and the resistivity anomaly in iron pnictides, Phys. Rev. B 80 (2009) 224506. doi:10.1103/PhysRevB.80.224506.

[28] C.-C. Lee, W.-G. Yin, W. Ku, Ferro-orbital order and strong magnetic anisotropy in the parent compounds of iron-pnictide superconductors, Phys. Rev. Lett. 103 (2009) 267001. doi:10.1103/PhysRevLett.103.267001.

[29] S. Onari, H. Kontani, Self-consistent vertex correction analysis for iron-based superconductors: Mechanism of coulomb interaction-driven orbital fluctuations, Phys. Rev. Lett. 109 (2012) 137001. doi:10.1103/PhysRevLett.109.137001.

[30] S. Raghu, A. Paramekanti, E. A. Kim, R. A. Borzi, S. A. Grigera, A. P. Mackenzie, S. A. Kivelson, Microscopic theory of the nematic phase in $Sr_3Ru_2O_7$, Phys. Rev. B 79 (2009) 214402. doi:10.1103/PhysRevB.79.214402.

[31] W.-C. Lee, C. Wu, Theory of unconventional metamagnetic electron states in orbital band systems, Phys. Rev. B 80 (2009) 104438. doi:10.1103/PhysRevB.80.104438.

[32] M. Tsuchiizu, Y. Ohno, S. Onari, H. Kontani, Orbital nematic instability in the two-orbital Hubbard model: Renormalization-group + constrained RPA analysis, Phys. Rev. Lett. 111 (2013) 057003. doi:10.1103/PhysRevLett.111.057003.

[33] D. Hirai, H. Sagayama, S. Gao, H. Ohsumi, G. Chen, T.-h. Arima, Z. Hiroi, Detection of multipolar orders in the spin-orbit-coupled $5d$ mott insulator Ba_2MgReO_6, Phys. Rev. Research 2 (2020) 022063. doi:10.1103/PhysRevResearch.2.022063.

[34] A. Mansouri Tehrani, N. A. Spaldin, Untangling the structural, magnetic dipole, and charge multipolar orders in Ba_2MgReO_6, Phys. Rev. Mater. 5 (2021) 104410. doi:10.1103/PhysRevMaterials.5.104410.

[35] S. W. Lovesey, D. D. Khalyavin, Magnetic order and $5d^1$ multipoles in a rhenate double perovskite Ba_2MgReO_6, Phys. Rev. B 103 (2021) 235160. doi:10.1103/PhysRevB.103.235160.

[36] M. Takigawa, H. Yasuoka, T. Tanaka, Y. Ishizawa, NMR study on the spin structure of CeB_6, J. Phys. Soc. Jpn. 52 (3) (1983) 728–731. doi:10.1143/JPSJ.52.728.

[37] H. Nakao, K.-i. Magishi, Y. Wakabayashi, Y. Murakami, K. Koyama, K. Hirota, Y. Endoh, S. Kunii, Antiferro-quadrupole ordering of CeB_6 studied by resonant X-ray scattering, J. Phys. Soc. Jpn. 70 (7) (2001) 1857–1860.

[38] Y. Tanaka, U. Staub, K. Katsumata, S. Lovesey, J. Lorenzo, Y. Narumi, V. Scagnoli, S. Shimomura, Y. Tabata, Y. Onuki, et al., Direct and quantitative determination of the orbital ordering in CeB_6 by X-ray diffraction, Europhys. Lett. 68 (5) (2004) 671. doi:10.1209/epl/i2004-10271-9.

[39] P. Y. Portnichenko, A. Akbari, S. E. Nikitin, A. S. Cameron, A. V. Dukhnenko, V. B. Filipov, N. Y. Shitsevalova, P. Čermák, I. Radelytskyi, A. Schneidewind, J. Ollivier, A. Podlesnyak, Z. Huesges, J. Xu, A. Ivanov, Y. Sidis, S. Petit, J.-M. Mignot, P. Thalmeier, D. S. Inosov, Field-angle-resolved magnetic excitations as a probe of hidden-order symmetry in CeB_6, Phys. Rev. X 10 (2020) 021010. doi:10.1103/PhysRevX.10.021010.

[40] P. Morin, D. Schmitt, E. D. T. De Lacheisserie, Magnetic and quadrupolar properties of $PrPb_3$, J. Magn. Magn. Mater. 30 (2) (1982) 257–264. doi:10.1016/0304-8853(82)90206-2.

[41] T. Onimaru, T. Sakakibara, A. Harita, T. Tayama, D. Aoki, Y. Ōnuki, Angle-resolved magnetization measurements on antiferroquadrupolar ordering system $PrPb_3$: Evidence for anisotropic quadrupolar interaction, J. Phys. Soc. Jpn. 73 (9) (2004) 2377–2380.

[42] T. Onimaru, T. Sakakibara, N. Aso, H. Yoshizawa, H. S. Suzuki, T. Takeuchi, Observation of modulated quadrupolar structures in $PrPb_3$, Phys. Rev. Lett. 94 (2005) 197201. doi:10.1103/PhysRevLett.94.197201.

[43] T. Onimaru, K. T. Matsumoto, Y. F. Inoue, K. Umeo, T. Sakakibara, Y. Karaki, M. Kubota, T. Takabatake, Antiferroquadrupolar ordering in a Pr-based superconductor $PrIr_2Zn_{20}$, Phys. Rev. Lett. 106 (2011) 177001. doi:10.1103/PhysRevLett.106.177001.

[44] I. Ishii, H. Muneshige, Y. Suetomi, T. K. Fujita, T. Onimaru, K. T. Matsumoto, T. Takabatake, K. Araki, M. Akatsu, Y. Nemoto, T. Goto, T. Suzuki, Antiferro-quadrupolar ordering at the lowest temperature and anisotropic magnetic field-temperature phase diagram in the cage compound $PrIr_2Zn_{20}$, J. Phys. Soc. Jpn. 80 (9) (2011) 093601. doi:10.1143/JPSJ.80.093601.

[45] A. Sakai, S. Nakatsuji, Kondo effects and multipolar order in the cubic $\mathrm{Pr}Tr_2\mathrm{Al}_{20}$ (Tr =Ti, V), J. Phys. Soc. Jpn. 80 (6) (2011) 063701. doi:10.1143/JPSJ.80.063701.

[46] T. Onimaru, H. Kusunose, Exotic quadrupolar phenomena in non-kramers doublet systems—the cases of $\mathrm{Pr}T_2\mathrm{Zn}_{20}$ (T = Ir, Rh) and $\mathrm{Pr}T_2\mathrm{Al}_{20}$ (T = V, Ti)—, J. Phys. Soc. Jpn. 85 (8) (2016) 082002. doi:10.7566/JPSJ.85.082002.

[47] T. Ishitobi, K. Hattori, Triple-q quadrupole-octupole order scenario for PrV_2Al_{20}, Phys. Rev. B 104 (2021) L241110. doi:10.1103/PhysRevB.104.L241110.

[48] H. Tanida, Y. Muro, T. Matsumura, La substitution and pressure studies on CeCoSi: A possible antiferroquadrupolar ordering induced by pressure, J. Phys. Soc. Jpn. 87 (2) (2018) 023705. doi:10.7566/JPSJ.87.023705.

[49] H. Tanida, K. Mitsumoto, Y. Muro, T. Fukuhara, Y. Kawamura, A. Kondo, K. Kindo, Y. Matsumoto, T. Namiki, T. Kuwai, T. Matsumura, Successive phase transition at ambient pressure in CeCoSi: Single crystal studies, J. Phys. Soc. Jpn. 88 (5) (2019) 054716. doi:10.7566/JPSJ.88.054716.

[50] M. Yatsushiro, S. Hayami, Odd-parity multipoles by staggered magnetic dipole and electric quadrupole orderings in CeCoSi, J. Phys. Soc. Jpn. 89 (1) (2020) 013703. doi:10.7566/JPSJ.89.013703.

[51] M. Manago, H. Kotegawa, H. Tou, H. Harima, H. Tanida, Unusual nonmagnetic ordered state in CeCoSi revealed by ^{59}Co-NMR and NQR measurements, J. Phys. Soc. Jpn. 90 (2) (2021) 023702. doi:10.7566/JPSJ.90.023702.

[52] H. Hidaka, S. Yanagiya, E. Hayasaka, Y. Kaneko, T. Yanagisawa, H. Tanida, H. Amitsuka, Magnetic field-temperature phase diagram of CeCoSi constructed on the basis of specific heat, magnetoresistivity, and magnetization measurements: Single crystal study, J. Phys. Soc. Jpn. 91 (9) (2022) 094701. doi:10.7566/JPSJ.91.094701.

[53] T. Matsumura, S. Kishida, M. Tsukagoshi, Y. Kawamura, H. Nakao, H. Tanida, Structural transition in the hidden ordered phase of CeCoSi, J Phys. Soc. Jpn. 91 (6) (2022) 064704. doi:10.7566/JPSJ.91.064704.

[54] M. Manago, A. Ishigaki, H. Tou, H. Harima, H. Tanida, H. Kotegawa, Ferroic quadrupolar ordering in CeCoSi revealed using ^{59}Co NMR measurements, Phys. Rev. B 108 (2023) 085118. doi:10.1103/PhysRevB.108.085118.

[55] J. Garaud, J. Carlström, E. Babaev, M. Speight, Chiral $\mathbb{C}P^2$ skyrmions in three-band superconductors, Phys. Rev. B 87 (2013) 014507. doi:10.1103/PhysRevB.87.014507.

[56] Y. Akagi, Y. Amari, N. Sawado, Y. Shnir, Isolated skyrmions in the CP^2 nonlinear sigma model with a Dzyaloshinskii-Moriya type interaction, Phys. Rev. D 103 (2021) 065008. doi:10.1103/PhysRevD.103.065008.

[57] Y. Amari, Y. Akagi, S. B. Gudnason, M. Nitta, Y. Shnir, $\mathbb{C}P^2$ skyrmion crystals in an SU(3) magnet with a generalized Dzyaloshinskii-Moriya interaction, Phys. Rev. B 106 (2022) L100406. doi:10.1103/PhysRevB.106.L100406.

[58] H. Zhang, Z. Wang, D. Dahlbom, K. Barros, C. D. Batista, CP^2 skyrmions and skyrmion crystals in realistic quantum magnets, Nat. Commun. 14 (2023) 3626.

[59] H. Tsunetsugu, T. Ishitobi, K. Hattori, Quadrupole orders on the fcc lattice, J. Phys. Soc. Jpn. 90 (4) (2021) 043701. doi:10.7566/JPSJ.90.043701.

[60] K. Hattori, T. Ishitobi, H. Tsunetsugu, Quadrupole partial orders and triple-$\mathbf{q}$ states on the face-centered cubic lattice, Phys. Rev. B 107 (2023) 205126. doi:10.1103/PhysRevB.107.205126.

[61] T. Ishitobi, K. Hattori, Triple-$\mathcal{Q}$ partial magnetic orders induced by quadrupolar interactions: Triforce order scenario for UNi_4B, Phys. Rev. B 107 (2023) 104413. doi:10.1103/PhysRevB.107.104413.

[62] S. Hayami, S. Tsutsui, H. Hanate, N. Nagasawa, Y. Yoda, K. Matsuhira, Cluster toroidal multipoles formed by electric-quadrupole and magnetic-octupole trimers: A possible scenario for hidden orders in $Ca_5Ir_3O_{12}$, J. Phys. Soc. Jpn. 92 (3) (2023) 033702. doi:https://doi.org/10.7566/JPSJ.92.033702.

[63] S. Hayami, Multiple-q instability under fourth-order inplane single-ion anisotropy, J. Magn. Magn. Mater. 570 (2023) 170507. doi:https://doi.org/10.1016/j.jmmm.2023.170507.

[64] S. Hayami, H. Kusunose, Microscopic description of electric and magnetic toroidal multipoles in hybrid orbitals, J. Phys. Soc. Jpn. 87 (3) (2018) 033709. doi:10.7566/JPSJ.87.033709.

[65] S. Hayami, M. Yatsushiro, Y. Yanagi, H. Kusunose, Classification of atomic-scale multipoles under crystallographic point groups and application to linear response tensors, Phys. Rev. B 98 (2018) 165110. doi:10.1103/PhysRevB.98.165110.

[66] H. Kusunose, S. Hayami, Generalization of microscopic multipoles and cross-correlated phenomena by their orderings, J. Phys.: Condens. Matter 34 (46) (2022) 464002. doi:10.1088/1361-648x/ac9209.

[67] H. Kusunose, R. Oiwa, S. Hayami, Complete multipole basis set for single-centered electron systems, J. Phys. Soc. Jpn. 89 (10) (2020) 104704. doi:10.7566/JPSJ.89.104704.

[68] H. Kusunose, R. Oiwa, S. Hayami, Symmetry-adapted modeling for molecules and crystals, Phys. Rev. B 107 (2023) 195118. doi:10.1103/PhysRevB.107.195118.

[69] S. Hayami, H. Kusunose, Y. Motome, Emergent spin-valley-orbital physics by spontaneous parity breaking, J. Phys.: Condens. Matter 28 (39) (2016) 395601. doi:10.1088/0953-8984/28/39/395601.

[70] S. Hayami, H. Kusunose, Essential role of the anisotropic magnetic dipole in the anomalous Hall effect, Phys. Rev. B 103 (2021) L180407. doi:10.1103/PhysRevB.103.L180407.

[71] S. Hayami, R. Oiwa, H. Kusunose, Electric ferro-axial moment as nanometric rotator and source of longitudinal spin current, J. Phys. Soc. Jpn. 91 (11) (2022) 113702. doi:10.7566/JPSJ.91.113702.

[72] S.-W. Cheong, F.-T. Huang, M. Kim, Linking emergent phenomena and broken symmetries through one-dimensional objects and their dot/cross products, Rep. Prog. Phys. 85 (2022) 124501. doi:10.1088/1361-6633/ac97aa.

[73] A. Kirikoshi, S. Hayami, Rotational response induced by electric toroidal dipole, J. Phys. Soc. Jpn. 92 (2023) 123703. doi:https://doi.org/10.7566/JPSJ.92.123703.

[74] I. Sodemann, L. Fu, Quantum nonlinear Hall effect induced by Berry curvature dipole in time-reversal invariant materials, Phys. Rev. Lett. 115 (2015) 216806. doi:10.1103/PhysRevLett.115.216806.

[75] S. Di Matteo, M. R. Norman, Nature of the tensor order in $\mathbf{Cd_2Re_2O_7}$, Phys. Rev. B 96 (2017) 115156. doi:10.1103/PhysRevB.96.115156.

[76] S. Hayami, Y. Yanagi, H. Kusunose, Y. Motome, Electric toroidal quadrupoles in the spin-orbit-coupled metal $Cd_2Re_2O_7$, Phys. Rev. Lett. 122 (2019) 147602. doi:10.1103/PhysRevLett.122.147602.

[77] T. Ishitobi, K. Hattori, Magnetoelectric effects and charge-imbalanced solenoids: Antiferro quadrupole orders in a diamond structure, J. Phys. Soc. Jpn. 88 (6) (2019) 063708. doi:10.7566/JPSJ.88.063708.

[78] S. Hayami, H. Kusunose, Chiral charge as hidden order parameter in URu_2Si_2, J. Phys. Soc. Jpn. 92 (2023) 113704. doi:https://doi.org/10.7566/JPSJ.92.113704.

[79] S. Hayami, M. Yatsushiro, Spin conductivity based on magnetic toroidal quadrupole hidden in antiferromagnets, J. Phys. Soc. Jpn. 91 (6) (2022) 063702. doi:10.7566/JPSJ.91.063702.

[80] S. Hayami, H. Kusunose, Time-reversal switching responses in antiferromagnets, Phys. Rev. B 108 (2023) L140409. doi:10.1103/PhysRevB.108.L140409.

[81] R. Shiina, H. Shiba, P. Thalmeier, Magnetic-field effects on quadrupolar ordering in a Γ 8-quartet system CeB_6, J. Phys. Soc. Jpn. 66 (6) (1997) 1741–1755. doi:10.1143/JPSJ.66.1741.

[82] O. Sakai, R. Shiina, H. Shiba, P. Thalmeier, A new interpretation of NMR in quadrupolar ordering phase of CeB_6-consistency with neutron scattering, J. Phys. Soc. Jpn. 66 (10) (1997) 3005–3007. doi:10.1143/JPSJ.66.3005.

[83] R. Shiina, O. Sakai, H. Shiba, P. Thalmeier, Interplay of field-induced multipoles in CeB_6, J. Phys. Soc. Jpn. 67 (3) (1998) 941–949. doi:10.1143/JPSJ.67.941.

[84] H. Shiba, O. Sakai, R. Shiina, Nature of Ce-Ce interaction in CeB_6 and its consequences, J. Phys. Soc. Jpn. 68 (6) (1999) 1988–1993. doi:10.1143/JPSJ.68.1988.

[85] O. Sakai, R. Shiina, H. Shiba, P. Thalmeier, Antiferro-polarization of octupolar moment in phase III of CeB_6-analysis of NMR spectra, J. Phys. Soc. Jpn. 68 (4) (1999) 1364–1370.

[86] T. Matsumura, T. Yonemura, K. Kunimori, M. Sera, F. Iga, Magnetic field induced $4f$ octupole in CeB_6 probed by resonant X-ray diffraction, Phys. Rev. Lett. 103 (2009) 017203. doi:10.1103/PhysRevLett.103.017203.

[87] T. Matsumura, T. Yonemura, K. Kunimori, M. Sera, F. Iga, T. Nagao, J.-i. Igarashi, Antiferroquadrupole order and magnetic field induced octupole in CeB_6, Phys. Rev. B 85 (2012) 174417. doi:10.1103/PhysRevB.85.174417.

[88] N. A. Spaldin, M. Fiebig, M. Mostovoy, The toroidal moment in condensed-matter physics and its relation to the magnetoelectric effect, J. Phys.: Condens. Matter 20 (43) (2008) 434203. doi:10.1088/0953-8984/20/43/434203.

[89] Y. V. Kopaev, Toroidal ordering in crystals, Physics-Uspekhi 52 (11) (2009) 1111–1125. doi:10.3367/UFNe.0179.200911d.1175.

[90] Y. Yanase, Magneto-electric effect in three-dimensional coupled zigzag chains, J. Phys. Soc. Jpn. 83 (1) (2014) 014703. doi:10.7566/JPSJ.83.014703.

[91] S. Hayami, H. Kusunose, Y. Motome, Spontaneous multipole ordering by local parity mixing, J. Phys. Soc. Jpn. 84 (6) (2015) 064717. doi:10.7566/JPSJ.84.064717.

[92] H. Watanabe, Y. Yanase, Nonlinear electric transport in odd-parity magnetic multipole systems: Application to Mn-based compounds, Phys. Rev. Research 2 (2020) 043081. doi:10.1103/PhysRevResearch.2.043081.

[93] M. Yatsushiro, R. Oiwa, H. Kusunose, S. Hayami, Analysis of model-parameter dependences on the second-order nonlinear conductivity in $\mathcal{PT}$-symmetric collinear antiferromagnetic metals with magnetic toroidal moment on zigzag chains, Phys. Rev. B 105 (2022) 155157. doi:10.1103/PhysRevB.105.155157.

[94] H. Watanabe, Y. Yanase, Magnetic hexadecapole order and magnetopiezoelectric metal state in $\mathbf{Ba}_{1-x}\mathbf{K}_x\mathbf{Mn}_2\mathbf{As}_2$, Phys. Rev. B 96 (2017) 064432. doi:10.1103/PhysRevB.96.064432.

[95] F. Thöle, N. A. Spaldin, Magnetoelectric multipoles in metals, Philos. Trans. R. Soc. A 376 (2134) (2018) 20170450. doi:10.1098/rsta.2017.0450.

[96] Y. Yanagi, S. Hayami, H. Kusunose, Manipulating the magnetoelectric effect: Essence learned from $Co_4Nb_2O_9$, Phys. Rev. B 97 (2018) 020404. doi:10.1103/PhysRevB.97.020404.

[97] S. Hayami, H. Kusunose, Y. Motome, Emergent odd-parity multipoles and magnetoelectric effects on a diamond structure: Implication for the $5d$ transition metal oxides $A\mathrm{OsO}_4$ ($A = \mathrm{K}, \mathrm{Rb}, \text{and Cs}$), Phys. Rev. B 97 (2018) 024414. doi:10.1103/PhysRevB.97.024414.

[98] S. Hayami, H. Kusunose, Spin-orbital-momentum locking under odd-parity magnetic quadrupole ordering, Phys. Rev. B 104 (2021) 045117. doi:10.1103/PhysRevB.104.045117.

[99] S. Hayami, M. Yatsushiro, H. Kusunose, Nonlinear spin Hall effect in $\mathcal{PT}$-symmetric collinear magnets, Phys. Rev. B 106 (2022) 024405. doi:10.1103/PhysRevB.106.024405.

[100] A. Kirikoshi, S. Hayami, Microscopic mechanism for intrinsic nonlinear anomalous Hall conductivity in noncollinear antiferromagnetic metals, Phys. Rev. B 107 (2023) 155109. doi:10.1103/PhysRevB.107.155109.

[101] S. Hayami, H. Kusunose, Y. Motome, Asymmetric magnon excitation by spontaneous toroidal ordering, J. Phys. Soc. Jpn. 85 (5) (2016) 053705. doi:10.7566/JPSJ.85.053705.

[102] V. M. Pergamenshchik, V. A. Uzunova, Dipolar colloids in nematostatics: Tensorial structure, symmetry, different types, and their interaction, Phys. Rev. E 83 (2011) 021701. doi:10.1103/PhysRevE.83.021701.

[103] V. Pergamenshchik, The model of elastic multipole, J. Mol. Liq. 267 (2018) 337–344.

[104] M. Yatsushiro, H. Kusunose, S. Hayami, Multipole classification in 122 magnetic point groups for unified understanding of multiferroic responses and transport phenomena, Phys. Rev. B 104 (2021) 054412. doi:10.1103/PhysRevB.104.054412.

[105] The expectation values of higher-rank multiples allowed from symmetry are omitted for simplicity.

[106] J.-I. Yamaura, Z. Hiroi, Low temperature symmetry of pyrochlore oxide $Cd_2Re_2O_7$, J. Phys. Soc. Jpn. 71 (11) (2002) 2598–2600. doi:10.1143/JPSJ.71.2598.

[107] H. T. Hirose, T. Terashima, D. Hirai, Y. Matsubayashi, N. Kikugawa, D. Graf, K. Sugii, S. Sugiura, Z. Hiroi, S. Uji, Electronic states of metallic electric toroidal quadrupole order in $Cd_2Re_2O_7$ determined by combining quantum oscillations and electronic structure calculations, Phys. Rev. B 105 (2022) 035116. doi:10.1103/PhysRevB.105.035116.

[108] D. Hirai, A. Fukui, H. Sagayama, T. Hasegawa, Z. Hiroi, Successive phase transitions of the spin–orbit-coupled metal $Cd_2Re_2O_7$ probed by high-resolution synchrotron x-ray diffraction, J. Phys.: Condens. Matter 51 (3) (2023) 035403. doi:10.1088/1361-648X/aca05e.

[109] W. Jauch, M. Reehuis, A. Schultz, γ-ray and neutron diffraction studies of CoF_2: magnetostriction, electron density and magnetic moments, Acta Crystallogr. A 60 (1) (2004) 51–57. doi:10.1107/s0108767303022803.

[110] S. Hayami, R. Yambe, H. Kusunose, Analysis of photo-induced chirality and magnetic toroidal moment based on floquet formalism, J. Phys. Soc. Jpn. 93 (4) (2024) 043702. doi:https://doi.org/10.7566/JPSJ.93.043702.